J. Fluid Mech. (2016), *vol.* 791, R2, doi:10.1017/jfm.2016.82

Moment generating functions and scaling laws in the inertial layer of turbulent wall-bounded flows

Xiang I. A. Yang[1,†], **Ivan Marusic**[2] **and Charles Meneveau**[1]

[1]Department of Mechanical Engineering, The Johns Hopkins University, Baltimore, MD 21218, USA

[2]Department of Mechanical Engineering, The University of Melbourne, Parkville, VIC 3010, Australia

Properties of single- and two-point moment generating functions (MGFs) are examined in the inertial region of wall-bounded flows. Empirical evidence for power-law scaling of the single-point MGF $\langle \exp(qu^+) \rangle$ (where u^+ is the normalized streamwise velocity fluctuation and q a real parameter) with respect to the wall-normal distance is presented, based on hot-wire data from a $Re_\tau = 13\,000$ boundary-layer experiment. The parameter q serves as a 'dial' to emphasize different parts of the signal such as high- and low-speed regions, for positive and negative values of q, respectively. Power-law scaling $\langle \exp(qu^+) \rangle \sim (z/\delta)^{-\tau(q)}$ can be related to the generalized logarithmic laws previously observed in higher-order moments, such as in $\langle u^{+2p} \rangle^{1/p}$, but provide additional information not available through traditional moments if considering q values away from the origin. For two-point MGFs, the scalings in $\langle \exp[qu^+(x) + q'u^+(x+r)] \rangle$ with respect to z and streamwise displacement r in the logarithmic region are investigated. The special case $q' = -q$ is of particular interest, since this choice emphasizes rare events with high and low speeds at a distance r. Applying simple scaling arguments motivated by the attached eddy model, a 'scaling transition' is predicted to occur for $q = q_{cr}$ such that $\tau(q_{cr}) + \tau(-q_{cr}) = 1$, where $\tau(q)$ is the set of scaling exponents for single-point MGFs. This scaling transition is not visible to traditional central moments, but is indeed observed based on the experimental data, illustrating the capabilities of MGFs to provide new and statistically robust insights into turbulence structure and confirming essential ingredients of the attached eddy model.

Key words: turbulent boundary layers, turbulent flows

† Email address for correspondence: xyang44@jhu.edu

1. Introduction and definitions

The topic of turbulent boundary layers has been one of the centrepieces of research in turbulent flows for many decades (Cebeci & Bradshaw 1977; Pope 2000; Schultz & Flack 2007; Smits, McKeon & Marusic 2011; Marusic *et al.* 2013). An important feature of wall boundary-layer flows is the logarithmic law (Prandtl 1925; von Kármán 1930) for the mean velocity profile $U/u_\tau \equiv U^+ = \kappa^{-1}\ln(zu_\tau/\nu) + B$ valid in the inertial region, where z is the distance to the wall, u_τ is the friction velocity based on the wall stress τ_w ($u_\tau = \sqrt{\tau_w/\rho}$, ρ is the fluid density), ν is the kinematic viscosity, κ is the von Kármán constant, and B is another constant (see results in Smits *et al.* (2011), Jiménez (2013), Marusic *et al.* (2013), Lee & Moser (2015) for recent empirical evidence for logarithmic scaling of the mean velocity). Even if only approximately valid under realistic conditions, such a basic property of wall-bounded turbulent flows continues to provide predictions in many practical applications, and it helps to test models, calibrate parameters, and guide the development of theories.

Recently, a logarithmic behaviour has also been observed in the inertial region for the variance of the fluctuations in the streamwise velocity component. Such behaviour can be motivated by model predictions based on the 'attached eddy hypothesis' by Townsend (1976) and Perry, Henbest & Chong (1986). There has been growing evidence (Marusic & Kunkel 2003; Hultmark *et al.* 2012) for a logarithmic behaviour of the form $\langle u^{+2}\rangle = B_1 - A_1\ln(z/\delta)$, where u^+ is the normalized streamwise velocity fluctuation and δ is an outer length scale. For developing boundary layers the outer scale is the boundary-layer thickness, while it is the radius for pipes, and the half-height for plane channels. Empirical data are mostly consistent with a value of $A_1 \approx 1.25$ (the Townsend–Perry constant), whereas B_1 is flow-dependent and thus not universal. The logarithmic structure extends to higher-order moments (Meneveau & Marusic 2013), and high-order structure functions also exhibit logarithmic behaviour in the relevant range of streamwise separation between two points (de Silva *et al.* 2015). Davidson, Nickels & Krogstad (2006) and Davidson & Krogstad (2014) describe relevant prior work on logarithmic scaling of second-order structure functions.

From the perspective of statistical descriptions of wall-bounded turbulence, high positive moments emphasize those intense events that deviate significantly from the mean. In fact, the most extreme value can be obtained from the limit of very high-order moments, since $\max(u) = \lim_{p\to+\infty}\langle u^p\rangle^{1/p}$. Those intense events, from a phenomenological perspective, can indicate the presence of certain flow structures, for example, high- and low-velocity streak structures that are known to be important in momentum transport in wall turbulence. However, moments do not provide a natural way to distinguish between the positive and negative fluctuations. Even-order moments mix the contributions from both positive and negative sides of the distribution. Odd-order moments emphasize the difference between the contributions of positive and negative fluctuations, which does not facilitate emphasizing positive and negative contributions separately. Conditional moments can be used for such discrimination, but they depend on both the threshold and the order of the moment, increasing complexity.

Another option to be explored here is provided by the exponential of the random variable of interest, and then considering various moments of this new random variable. More specifically, considering streamwise velocity fluctuations in a boundary layer at a height z, and point-pair distances r in the streamwise direction, we consider the following statistical objects:

$$W(q; z) \equiv \langle \exp(q\,u^+)\rangle, \quad W(q, q'; z, r) \equiv \langle \exp[q\,u^+(x) + q'\,u^+(x+r)]\rangle. \qquad (1.1a,b)$$

These are the single- and two-point moment generating functions (MGFs), respectively. The parameter q, a real number, serves as a 'dial' to emphasize different parts of the signal, such as high- and low-speed regions, for positive and negative values of q, respectively. For two-point statistics, choosing different values of q and q' enables one to emphasize particular behaviours at points separated by a distance r. One natural consequence of the definition of MGFs is that single- and two-point moments can be directly computed from the curvatures of the MGFs at the origin, according to

$$\left.\begin{aligned} \langle u^{+p}\rangle &= \left.\frac{\partial^p W(q;z)}{\partial q^p}\right|_{q=0}, \\ \langle u^+(x)^p u^+(x+r)^{p'}\rangle &= \left.\frac{\partial^{p'}}{\partial q'^{p'}}\frac{\partial^p}{\partial q^p}W(q,q';z,r)\right|_{q=0,q'=0}. \end{aligned}\right\} \tag{1.2}$$

It is worth noting here that central moments are solely determined by the moment generating function at $q=0$.

It is also useful to mention that $W(q;z)$ as defined corresponds to a highly simplified and real-valued subset of the more general object described by the Hopf equation (Hopf 1952; Monin & Yaglom 2007). This equation describes the full N-point joint PDF of velocity fluctuations, where N is the total number of different spatial points needed to describe the flow. Basic interest in the Hopf equation follows from the fact that it is a linear equation, and therefore self-contained, requiring no closure. It describes the time evolution of the generalized moment generating function $\Psi(\boldsymbol{\theta}) = \langle \exp(\mathrm{i}\int \boldsymbol{\theta}(\boldsymbol{x}) \cdot \boldsymbol{u}(\boldsymbol{x})\,\mathrm{d}^3\boldsymbol{x})\rangle$, where $\boldsymbol{u}$ is the velocity field, $\mathrm{i}\boldsymbol{\theta}(\boldsymbol{x})$ is a complex 'test field' which serves as a (very high-dimensional) independent variable taking on specified values at every point in the flow. As mentioned before, the Hopf equation is a linear equation for $\Psi(\boldsymbol{\theta})$. However, it includes functional derivatives with respect to the entire test field $\boldsymbol{\theta}(\boldsymbol{x})$, and solving such functional equations remains an unattainable theoretical goal. The new quantity $W(q;z)$ may be considered to be a highly simplified version, a 'subset', of $\Psi(\boldsymbol{\theta})$ in which we take a special-case test field $\mathrm{i}\theta_j(\boldsymbol{x}) = q\delta(\boldsymbol{x}-z\hat{\boldsymbol{k}})\delta_{j1}$, and similarly for the two-point MGF $\mathrm{i}\theta_j(\boldsymbol{x}) = q\delta(\boldsymbol{x}-z\hat{\boldsymbol{k}})\delta_{j1} + q'\delta(\boldsymbol{x}-r\hat{\boldsymbol{i}}-z\hat{\boldsymbol{k}})\delta_{j1}$ (where $\hat{\boldsymbol{k}}$ and $\hat{\boldsymbol{i}}$ are the unit vectors in the wall-normal and streamwise directions, respectively).

Another connection with prior approaches can be highlighted. In the study of small-scale intermittency and anomalous scaling, high-order moments of turbulent kinetic energy dissipation normalized by its mean, $\varepsilon/\langle\varepsilon\rangle$, such as $\langle(\varepsilon/\langle\varepsilon\rangle)^q\rangle$ with $q>0$, are used to emphasize the highly intermittent peaks in dissipation, while the low-dissipation regions can be highlighted by moments of negative order $q<0$ (see e.g. Meneveau & Sreenivasan 1991; O'Neil & Meneveau 1993; Frish 1995). The analogy is then between u^+ and the variable $\ln(\varepsilon/\langle\varepsilon\rangle)$. As will be seen in the discussion in §§ 2 and 3, an analogy between the momentum cascade and the energy cascade can be formally made, providing helpful insights for the study of wall-bounded flows (see also Jiménez 2011).

The discussion here focuses on boundary-layer flows. For the variance of the streamwise velocity fluctuations to exhibit logarithmic scaling one may hypothesize that $\langle\exp(qu^+)\rangle$ exhibits power-law scaling with respect to z near $q=0$, since

$$W(q;z) \sim \left(\frac{z}{\delta}\right)^{-\tau(q)} \rightarrow \langle u^{+2}\rangle = \left.\frac{\partial^2 W(q;z)}{\partial q^2}\right|_{q=0} = B_2 - \left.\frac{\mathrm{d}^2\tau(q)}{\mathrm{d}q^2}\right|_{q=0}\log\left(\frac{z}{\delta}\right). \tag{1.3}$$

However, the known logarithmic behaviour of $\langle u^{+2}\rangle$ does not imply power-law scaling of $W(q; z)$ for q values away from $q = 0$, so this must be tested based on data.

The rest of the paper is organized as follows: the scaling behaviour of the single-point MGF is investigated in § 2, including empirical evidence of power-law scaling as a function of height z, for q both positive and negative. Experimental measurements of flow at $Re_\tau \approx 13\,000$ from the Melbourne High Reynolds Number Boundary Layer Wind Tunnel (HRNBLWT) are considered for this purpose. In § 3, we consider two-point MGFs and, in particular, provide an 'attached eddy' model based prediction of a scaling transition for $W(q, -q; z, r)$. This behaviour is confirmed by analysis of experimental data. Statistical convergence of the data is examined in § 4, and conclusions are provided in § 5. Throughout the paper, u^+ is the streamwise velocity fluctuation normalized by friction velocity and z is the wall-normal coordinate. The overall picture of wall-bounded flows provided by the Townsend attached eddy hypothesis (Townsend 1976) is found useful in the discussion and is often invoked (or implied). In Townsend (1976), as well as in Perry & Chong (1982) and Woodcock & Marusic (2015), the boundary layer is hypothesized to consist of attached eddies whose sizes scale with their distance from the wall and whose population density scales inversely with distance from the wall.

2. Scaling of single-point MGFs

We present results of the MGFs from high-Reynolds-number boundary-layer turbulence. Hot-wire streamwise velocity measurements at $Re_\tau = 13\,000$ from the Melbourne HRNBLWT are analysed (with $U_\infty = 20$ (m s^{-1}), $u_\tau = 0.639$ (m s^{-1}) and $\delta = 0.319$ (m), see Marusic *et al.* (2015) for further details of the dataset). The MGFs are computed for various q values in a range between ± 2. Statistics are evaluated at the 50 measurement heights averaging over a time interval of approximately $T_{data} = 11\,200\delta/U_\infty$. The measured MGFs as function of wall distance in inner units are shown in figure 1(*a*) for representative values of q. In the range $610 < z^+$, $z < 0.2\delta$ (see Marusic *et al.* (2013) for detailed discussion on the range of the log layer), power-law behaviour is observed. Moreover, there is significant difference in the scaling exponents of $W(q; z)$ for positive and negative q values of the same magnitude. This is especially the case for high $|q|$. The respective scaling ranges differ depending on the sign of q: for $q > 0$, the power-law region extends down to heights $z^+ \approx 400$, while for $q < 0$, the power-law region is shorter, down only to wall distances of about $z^+ \approx 600$. Note that $z^+ \approx 400$ corresponds nominally to the lower limit $3Re_\tau^{0.5}$ identified in Marusic *et al.* (2013) as appropriate for the logarithmic scaling range of the variance. This appears appropriate for the $q > 0$ cases, but for $q < 0$, the range is more consistent with $z^+ = 600$. Since negative q emphasizes the scaling behaviour of the low-speed regions of the flow, it is concluded that these are affected by wall and viscous effects up to larger distances from the wall, consistent with those regions being associated more prevalently with positive vertical velocities.

Equation (1.3) suggests power scaling of $W(q; z)$ near $q = 0$ and for z values where the $\langle u^{+2}\rangle$ has logarithmic scaling. Such scaling can also be obtained by considering the velocity fluctuations as resulting from a sum of discrete random contributions from attached eddies:

$$u^+ = \sum_{i=1}^{N_z} a_i. \tag{2.1}$$

Here the a_i are random additives, assumed to be identically and independently distributed, each associated with an attached eddy of size $\sim\delta/2^i$ if for simplicity we

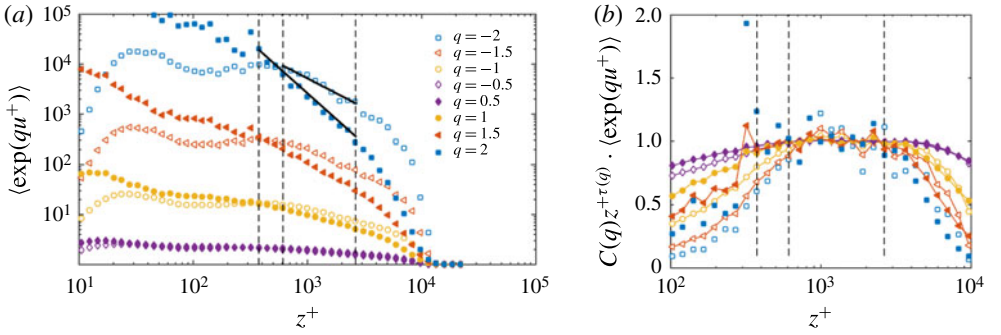

FIGURE 1. (*a*) Log–log plot of $\langle \exp(qu^+) \rangle$ against z^+ for $q = \pm 0.5, \pm 1, \pm 1.5, \pm 2$. Solid symbols are used for positive q values and hollow symbols are used for negative q values. The extent of the scaling regions, $375 < z^+$, $z < 0.2\delta$ for $q > 0$ and $610 < z^+$, $z < 0.2\delta$ for $q < 0$ are indicated by vertical dashed lines. (*b*) Premultiplied single-point MGF, $C(q)z^{+\tau(q)} \cdot \langle \exp(qu^+) \rangle$. The prefactor $C(q)$ is determined from the power-law fitting (such that in the fitted range $C(q)z^{+-\tau(q)} \approx \langle \exp(qu^+) \rangle$). Values of $\tau(q)$ used in the premultiplied quantities are $\tau = 0.17,\ 0.54,\ 0.91,\ 1.18$ for $q = -0.5,\ -1,\ -1.5,\ -2$ and $\tau = 0.17,\ 0.63,\ 1.27,\ 2.04$ for $q = 0.5,\ 1,\ 1.5,\ 2$.

choose a scale ratio of 2. The number of additives N_z is taken to be proportional to the number of attached eddies at any given height z. If the eddy population density is inversely proportional to z according to the attached eddy hypothesis (Townsend 1976), then N_z is proportional to:

$$N_z \sim \int \frac{1}{z}\,\mathrm{d}z \sim \log\left(\frac{\delta}{z}\right). \tag{2.2}$$

As a result, the exponential moment can be evaluated

$$\langle \exp(qu^+) \rangle = \langle \exp(qa) \rangle^{N_z} = \left(\frac{z}{\delta}\right)^{-C_e \log\langle \exp(qa) \rangle}, \tag{2.3}$$

where C_e is some constant. Equation (2.3) provides a prediction for the scaling exponents $\tau(q)$:

$$\tau(q) = C_e \log\langle \exp(qa) \rangle. \tag{2.4}$$

$\tau(q)$ is determined by the probability density function (p.d.f.) of the random additives a, representing the velocity field induced by a typical attached eddy. If these eddies are assumed to be purely inertial without dependence on viscosity, then $\tau(q)$ would be expected to be independent of Reynolds number. Furthermore, if a is assumed to be a Gaussian variable, then (2.4) leads to the quadratic law

$$\tau(q) = Cq^2, \tag{2.5}$$

where C is another constant. In order to compare this behaviour with measurements, we fit $\tau(q)$ from data (as shown in figure 1*a*) in the relatively narrow and conservative range $600 < z^+$, $z < 0.2\delta$, the common range where both positive and negative q display good scaling. The quality of the power-law fitting is further examined in figure 1(*b*), where the premultiplied single-point MGFs are plotted against the

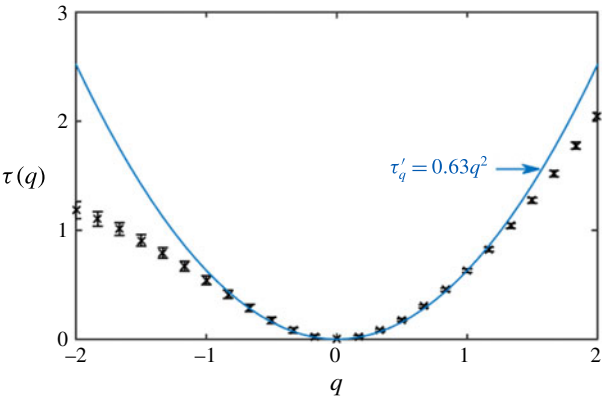

FIGURE 2. Measured scaling exponents $\tau(q)$ (symbols), obtained from fitting $W(q; z)$ as a function of z, in the range $610 < z^+$ and $z < 0.2\delta$. Error bars show the uncertainty in the obtained exponents. A quadratic fit around the origin yields $\tau(q) = 0.63q^2$ (blue solid line).

wall-normal distance. The fitted $\tau(q)$ curve is plotted against q in figure 2, including error bars determined by the ratio of the root mean square of the variation in $\log(\exp(qu^+)) - \tau(q)\log(z^+)$ in the fitted range of z^+ to the corresponding expected increase (or decrease) in $\langle \exp(qu^+)\rangle$ indicated by the fitted parameter. Due to statistical convergence issues, evaluation of $\tau(q)$ is limited to $|q| < 2$. A quadratic fit around $q = 0$ is shown with the solid line in figure 2. The fit yields $\tau(q) = 0.63q^2$. According to (1.3),

$$A_1 = \left.\frac{\mathrm{d}^2\tau(q)}{\mathrm{d}q^2}\right|_{q=0} = 2C = 1.26. \tag{2.6}$$

This is consistent with the prior measurements of the 'Perry–Townsend' constant $A_1 \approx 1.25$ (Hultmark *et al.* 2012; Marusic *et al.* 2013; Meneveau & Marusic 2013). Studying possible Reynolds number effects falls beyond the scope of this paper.

We can also compute $\langle u^{+2p}\rangle^{1/p}$ using the single-point MGF $\langle \exp(qu^+)\rangle$. Equations (1.2), (1.3) and (2.5) lead to $\langle u^{+2}\rangle = 1 \times 2C\log(\delta/z)$, $\langle u^{+4}\rangle^{1/2} = 3^{1/2} \times 2C\log(\delta/z)$, $\langle u^{+6}\rangle^{1/3} = 15^{1/3} \times 2C\log(\delta/z)$ and $\langle u^{+8}\rangle^{1/4} = 105^{1/4} \times 2C\log(\delta/z)$, recovering the scaling of generalized logarithmic laws (Meneveau & Marusic 2013). Because of the Gaussianity that underlies (2.5), it is not surprising that $A_p/A_1 = [(2p-1)!!]^{1/p}$ (see Meneveau & Marusic 2013; Woodcock & Marusic 2015). But, as can be discerned in figure 2, the quadratic fit becomes highly inaccurate away from $q = 0$, consistent with known deviations from Gaussian behaviour of velocity fluctuations in wall boundary-layer turbulence. Also the data are asymmetric, showing significantly stronger deviations from the Gaussian prediction for $q < 0$ than for $q > 0$. These results constitute new information about the flow and may prove important in comparing with models.

3. Two-point MGFs and scaling transition

In this section, the scaling behaviour of the two-point moment generating function $W(q, q'; z, r) = \langle \exp[qu^+(x, z) + q'u^+(x + r, z)]\rangle$ in the logarithmic region (for moments as function of z) and in the relevant range of the two-point separation distance r

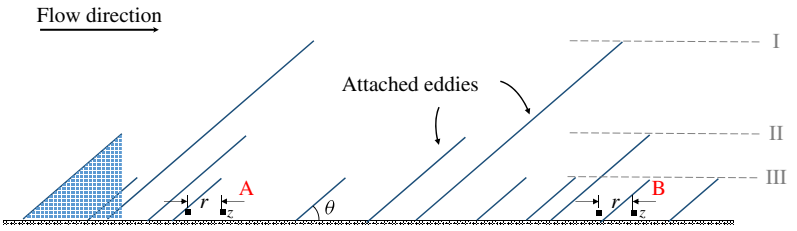

FIGURE 3. Conceptual sketch of a boundary layer with three hierarchies of attached eddies (I, II, III). $\theta \approx 17^\circ$ is the inclination angle of a typical attached eddy; consistent with a packet structure (Woodcock & Marusic 2015). Both points in set A as well as in set B are at a height z above the wall and are separated by a distance r in the flow direction. An attached eddy affects the region beneath it, as is indicated by the shaded region (Townsend 1976).

is investigated. Note that here we indicate z explicitly to avoid confusion. Before analysing the data, predictions of scaling behaviour exploiting the assumed hierarchical tree structure of attached eddies are presented. Figure 3 shows a sketch of attached eddies. We consider two points at a wall distance z that are separated by a distance r in the flow (x) direction. Velocity fluctuations at the two points are given by the random additives a_i corresponding to all the eddies 'above' a given point. As a result, two points at a distance r will share a subset of common additives from the larger eddies that contain both points, while each contains independent additives from eddies that are not common to both points. This consideration then enables one to factor the exponentials to separate common and separate contributions. The approach follows that of Meneveau & Chhabra (1990) and O'Neil & Meneveau (1993) who considered such factorizations of two-point moments of dissipation rate, and a crucial concept is that of the size of the smallest common eddy, r_c. To find the scaling for $W(q, q'; z, r)$, the quantity $\exp(qu^+(x, z) + q'u^+(x + r, z))$ is conditioned based on the size of the smallest common eddy r_c of the points under consideration, and the final result is given by the sum over all possible common eddy sizes r_c:

$$W(q, q'; z, r) = \sum_{r_c=r}^{\delta/\tan\theta} \langle \exp[qu^+(x, z)] \exp[q'u^+(x + r, z)] \mid r_c \rangle P_{r_c}, \tag{3.1}$$

where P_{r_c} is the probability that the smallest common eddy shared by the two points (x, z), $(x + r, z)$ is of size r_c. Eddies of size larger than r_c affect both points equally.

Also, we make the association that an eddy size of r_c in the horizontal direction has a height $z_c = r_c \tan\theta$. Factorizing the exponential at both points to contributions from eddies of size larger than r_c (heights above z_c) and eddies smaller than r_c (heights less than z_c) leads to

$$\langle \mathrm{e}^{qu^+(x,z)+q'u^+(x+r,z)} \mid r_c \rangle = \left\langle \mathrm{e}^{(q+q')u^+(x,z_c)} \frac{\mathrm{e}^{qu^+(x,z)}}{\mathrm{e}^{qu^+(x,z_c)}} \frac{\mathrm{e}^{q'u^+(x+r,z)}}{\mathrm{e}^{q'u^+(x+r,z_c)}} \middle| r_c \right\rangle. \tag{3.2}$$

Eddies of size smaller than r_c cannot affect both points at the same time, therefore the differences $u^+(x, z) - u^+(x, z_c)$ and $u^+(x + r, z) - u^+(x + r, z_c)$ (or the ratio of the exponentials), which according to the random additive ansatz (2.1) contain only contributions (additives) from eddies of size smaller than r_c, can be assumed to be

statistically independent. Also, they are independent of the additives corresponding to the velocity difference $u^+(x,\delta)-u^+(x,z_c)$. These arguments lead to

$$\langle \mathrm{e}^{qu^+(x,z)+q'u^+(x+r,z)} \mid r_c\rangle = \langle \mathrm{e}^{(q+q')u^+(x,z_c)}\rangle \left\langle \frac{\mathrm{e}^{qu^+(x,z)}}{\mathrm{e}^{qu^+(x,z_c)}}\right\rangle \left\langle \frac{\mathrm{e}^{q'u^+(x+r,z)}}{\mathrm{e}^{q'u^+(x+r,z_c)}}\right\rangle . \tag{3.3}$$

Following the same arguments that lead to (2.3), we have

$$\left\langle \frac{\mathrm{e}^{qu^+(x,z)}}{\mathrm{e}^{qu^+(x,z_c)}}\right\rangle \sim \left(\frac{z_c}{z}\right)^{\tau(q)} \tag{3.4}$$

and similarly at $x+r$ involving $\tau(q')$. Substituting (3.4) into (3.2) leads to

$$\langle \mathrm{e}^{qu^+(x,z)+q'u^+(x+r,z)} \mid r_c\rangle \sim P_{r_c}\left(\frac{z}{z_c}\right)^{-\tau(q)-\tau(q')}\left(\frac{z_c}{\delta}\right)^{-\tau(q+q')}. \tag{3.5}$$

To estimate P_{r_c} for some height z, we follow Meneveau & Chhabra (1990) and O'Neil & Meneveau (1993), and argue that P_{r_c} is proportional to the area of a strip of thickness r along the perimeter of an eddy of size r_c (area $\sim r\,r_c$), divided by the total area of such an eddy in the plane ($\sim r_c^2$). For point pairs falling within such a strip, the two points typically pertain to different eddies of size r_c. Hence $P_{r_c}\sim r/r_c$, and after replacing $z_c = r_c\tan\theta$, we can write

$$\langle \mathrm{e}^{qu^+(x,z)+q'u^+(x+r,z)}\rangle \sim \sum_{r_c=r}^{\delta/\tan\theta}\left(\frac{r_c}{\delta}\right)^{\tau(q)+\tau(q')-\tau(q+q')-1}\left(\frac{r}{\delta}\right)\left(\frac{z}{\delta}\right)^{-\tau(q)-\tau(q')}, \tag{3.6}$$

where a prefactor depending on $\tan\theta$ has been omitted for simplicity. At high Reynolds numbers, we can consider the situation $\delta/\tan\theta \gg r$. Thinking in terms of a discrete hierarchy of eddies, the sum in (3.6) becomes a geometric one. It is dominated either by the value at small scales $r_c\sim r$ or at large scales $r_c\sim\delta/\tan\theta$, depending on the sign of the exponent. Therefore, two asymptotic regimes can then be identified:

$$\left.\begin{array}{ll} W(q,q';z,r)\sim (z/\delta)^{-\tau(q)-\tau(q')}(r/\delta)^{\tau(q)+\tau(q')-\tau(q+q')}, & \text{if } \tau(q)+\tau(q')-\tau(q+q')-1<0,\\ W(q,q';z,r)\sim (z/\delta)^{-\tau(q)-\tau(q')}(r/\delta)^{1}, & \text{if } \tau(q)+\tau(q')-\tau(q+q')-1>0, \end{array}\right\} \tag{3.7}$$

indicating a 'scaling transition' with respect to r when q and q' are such that $\tau(q)+\tau(q')-\tau(q+q')-1=0$.

To examine whether such a scaling transition exists in the measurements, we consider the specific case $q'=-q$, for which the predicted scaling behaviour with respect to r is:

$$W(q,-q;z,r)\sim\left(\frac{r}{\delta}\right)^{\Phi(q)}, \quad \text{where } \Phi(q)=\min[\tau(q)+\tau(-q),1], \tag{3.8}$$

since $\tau(0)=0$ by construction. It is worth noting here that such a scaling transition is indicative of the 'tree-like' or hierarchical and space-filling structure on which the attached eddies are organized and, since the transition occurs away from $q=0$, it cannot be diagnosed using traditional two-point moments.

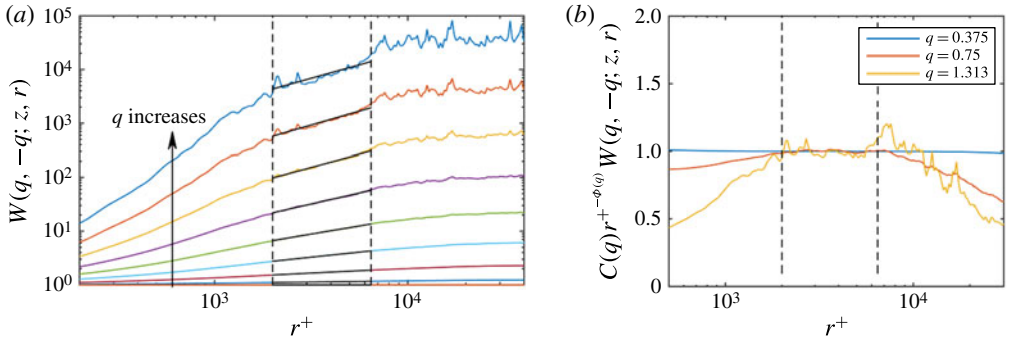

FIGURE 4. Log–log plot of $W(q, -q; z, r)$ against r at $z^+ = 600$, for nine values of q ranging from 0 to 1.5 (shown values are $q = 0$, 0.188, 0.375, 0.563, 0.75, 0.938, 1.125, 1.313 and 1.5). The range of r chosen to determine the power-law scaling exponent (relevant for the log region) is $z/\tan\theta$, to $0.15\delta/\tan\theta$. At $z^+ = 600$, this range corresponds to (approximately) $2000 < r^+ < 6500$. This range is indicated by two thin dashed vertical lines. The fits are indicated by solid lines. (*b*) Premultiplied two-point MGFs $C(q)r^{+-\Phi(q)}W(q, -q; z, r)$ for representative q values. The prefactor $C(q)$ is determined from the power-law fitting. $\Phi(q)$ used in the premultiplied quantities are 0.18, 0.61, 1.04 for q being 0.375, 0.75, 1.313.

Based on the dataset described before, $W(q, -q; z, r)$ is evaluated and plotted against r^+ in figure 4(*a*) for a specific wall-normal position in the log region (here taken at $z^+ = 600$) and for various values of q. We evaluate two-point correlations using direct summation (and checked that FFT gives essentially the same results). The relevant range in r for the scaling predicted in (3.7) is between $r = z/\tan(\theta)$ (any r below this value corresponds to eddies of size smaller than z and is thus not relevant) and $0.15\delta/\tan\theta$ (this is more conservative compared to $0.2\delta/\tan\theta$). For the specific height considered in figure 4, this range corresponds to $2000 < r^+ < 6500$ and is indicated by the dashed vertical lines. As can be seen, $W(q, -q; z, r)$ does exhibit power-law scaling in the relevant range of r. The quality of the power-law fitting is further examined in figure 4(*b*), where the premultiplied two-point MGFs are plotted against the two-point distance r^+. Moreover, as is already clear in figure 4(*a*), the scaling exponent gradually increases as q increases, but then the slope ceases to increase further with increasing q. We fit for $\Phi(q)$ in the range of r indicated by the two vertical dashed lines in figure 4. Figure 5 compares the measured $\Phi(q)$ and the prediction made in (3.8). Measured values for $\tau(q)$ and $\tau(-q)$ are used in (3.8). As can be seen from figure 5, a scaling transition exists and it appears to be correctly predicted by the scaling analysis leading to (3.7). The error bars for the fitted slopes are estimated as the ratio of the root mean square of the variations in $\log(W(q, -q; z, r)) - \Phi(q)\log(r)$ in the fitting range of r to the expected change indicated by the fitted parameter, i.e. error = r.m.s.$[\log(W(q, -q; z, r)) - \Phi(q)\log(r)]/(\Phi(q)\log(\Delta r))$, where Δr is range of r used in fitting.

Furthermore, the scaling of $W(q, q'; z, r)$ can be used to compute general moments such as $\langle u^m(x, z)u^n(x + r, z)\rangle$ and $\langle(u(x, z) - u(x + r, z))^{2n}\rangle$ (the latter are simply combinations of $\langle u_z^m(x)u_z^n(x+r)\rangle$). As an example, we compute $\langle u^+(x)u^+(x+r)\rangle$ using (1.2), (3.7):

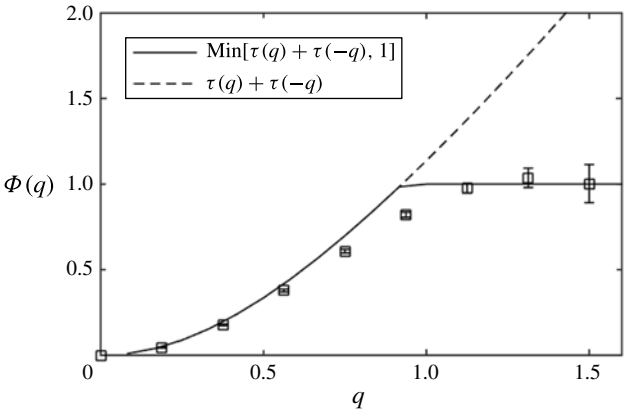

FIGURE 5. A comparison of the experimental measurements and model predictions of $\Phi(q)$ (symbols and solid line) against q. $\Phi(q)$ is the exponent on r in the predicted scaling behaviour of $W(q, -q; z, r)$.

$$\langle u^+(x)u^+(x+r)\rangle = \frac{\partial}{\partial q}\frac{\partial}{\partial q'}\langle \mathrm{e}^{qu^+(x)+q'u^+(x+r)}\rangle\bigg|_{q=q'=0} = 2C\log(r/\delta) = A_1\log(r/\delta). \quad (3.9)$$

This logarithmic scaling is not unexpected since it is consistent with the -1 power law in the energy spectrum. With $\langle u^+(x)u^+(x+r)\rangle$ known, we can compute the structure function as

$$\langle (u^+(x)-u^+(x+r))^2\rangle = 2\langle u^{+2}\rangle - 2\langle u^+(x)u^+(x+r)\rangle = 2A_1\log\left(\frac{r}{z}\right). \quad (3.10)$$

This recovers the observation made in de Silva *et al.* (2015). Higher-order structure functions can be calculated and logarithmic scalings can be recovered within in this framework (not shown here for succinctness).

4. Data convergence

Statistical convergence of the statistical moments measured in this work can be verified by examining the premultiplied probability density function (p.d.f.). In particular, we examine $\mathrm{e}^{\pm u^+}P(u^+)$ and $\mathrm{e}^{\pm 2u^+}P(u^+)$, where $P(u^+)$ is the single-point p.d.f. of the velocity at a representative wall-normal height $z^+ = 610$ (which is above $3Re^{0.5}$ and is still deep into the log region). For the two-point MGF considered in § 3, we evaluate the two-point joint p.d.f. $P(u_1, u_2)$ where u_1 and u_2 are velocities at two points x and $x+r$, and examine the quantity $L(u_1)$ defined as

$$L(u_1) = \exp(qu_1)\int_{u_2}\exp(-qu_2)P(u_1, u_2)\,\mathrm{d}u_2. \quad (4.1)$$

Since $W(q, -q; z, r) = \int L(u_1)\,\mathrm{d}u_1$, examination of the tails of $L(u_1)$ provides information about statistical convergence in measurements of $W(q, -q; z, r)$. We examine $L(u_1)$ at the same wall-normal height $z^+ = 610$ and a representative $r^+ = 2500$ (which is within the relevant range $z/\tan\theta < r < 0.15\delta/\tan\theta$).

As can be seen in figure 6, the quantities of interest, i.e. $\langle \mathrm{e}^{qu^+}\rangle$ and $\langle \mathrm{e}^{q(u^+(x)-u^+(x+r))}\rangle$, which are equal to the area under these curves, are well captured by the data available,

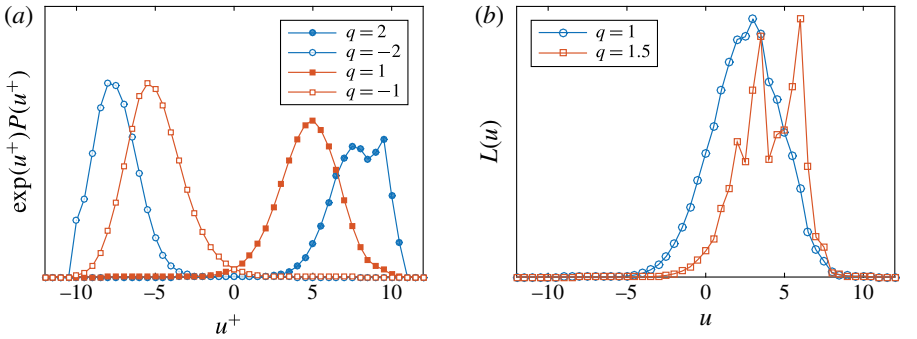

FIGURE 6. Premultiplied p.d.f. $\exp(u^+)P(u^+)$ (*a*) and $L(u)$ (*b*).

at least for those q values considered in §§ 2 and 3. Additionally, these figures illustrate the properties of MGFs that, by raising $\exp(u^+)$ to positive or negative powers, regions of high or low velocity are highlighted respectively (as is seen in figure 6*a*) and show distinctly asymmetric behaviour.

5. Conclusions

Introducing a new framework for the study of turbulence statistics in the logarithmic region in boundary layers, basic properties of the single-point and two-point moment generating function have been investigated. Power-law behaviours are observed in relevant ranges of z and r (the latter for two-point moment generating functions) during analysis of experimental measurements. By taking negative or positive values of the parameter q, the single-point moment generating function $W(q; z)$ can be used to investigate separately the properties of low-velocity regions and high-velocity regions. Such distinctions are not easily accessible when using traditional moments. A scaling transition in the two-point MGF, $W(q, -q; z, r)$, is predicted based on a simplified model inspired by the attached eddy hypothesis. Such a transition is indeed observed in the measurements and provides quantifiable evidence that the attached eddies through the log region are organized in a 'tree-like' or hierarchical and space-filling manner. Such an organization was assumed in previous attached eddy modelling efforts (Woodcock & Marusic 2015). Deviations from Gaussian statistics are visible in the scaling behaviour of the MGFs for q away from $q = 0$. Various turbulence statistics can be derived from the MGFs and known logarithmic scaling laws in single-point even-order moments and structure functions can be recovered.

Acknowledgements

The authors gratefully acknowledge the financial support of the Office of Naval Research, the National Science Foundation, and the Australian Research Council.

References

CEBECI, T. & BRADSHAW, P. 1977 *Momentum Transfer in Boundary Layers*. Hemisphere.

DAVIDSON, P. & KROGSTAD, P.-Å. 2014 A universal scaling for low-order structure functions in the log-law region of smooth-and rough-wall boundary layers. *J. Fluid Mech.* **752**, 140–156.

DAVIDSON, P., NICKELS, T. & KROGSTAD, P.-Å. 2006 The logarithmic structure function law in wall-layer turbulence. *J. Fluid Mech.* **550**, 51–60.

FRISH, U. 1995 *Turbulence: The Legacy of an Kolmogorov*. Cambridge University Press.

HOPF, E. 1952 Statistical hydromechanics and functional calculus. *J. Ration. Mech. Anal.* **1** (1), 87–123.

HULTMARK, M., VALLIKIVI, M., BAILEY, S. & SMITS, A. 2012 Turbulent pipe flow at extreme Reynolds numbers. *Phys. Rev. Lett.* **108** (9), 094501.

JIMÉNEZ, J. 2011 Cascades in wall-bounded turbulence. *Annu. Rev. Fluid Mech.* **44** (1), 27–45.

JIMÉNEZ, J. 2013 Near-wall turbulence. *Phys. Fluids* **25** (10), 101302.

VON KÁRMÁN, T. 1930 Mechanische änlichkeit und turbulenz. *Nachrichten von der Gesellschaft der Wissenschaften zu Göttingen, Mathematisch-Physikalische Klasse* **1930**, 58–76.

LEE, M. & MOSER, R. D. 2015 Direct numerical simulation of a turbulent channel flow up to $Re_\tau = 5200$. *J. Fluid Mech.* **774**, 395–415.

MARUSIC, I., CHAUHAN, K., KULANDAIVELU, V. & HUTCHINS, N. 2015 Evolution of zero-pressure-gradient boundary layers from different tripping conditions. *J. Fluid Mech.* **783**, 379–411.

MARUSIC, I. & KUNKEL, G. J. 2003 Streamwise turbulence intensity formulation for flat-plate boundary layers. *Phys. Fluids* **15** (8), 2461–2464.

MARUSIC, I., MONTY, J. P., HULTMARK, M. & SMITS, A. J. 2013 On the logarithmic region in wall turbulence. *J. Fluid Mech.* **716**, R3.

MENEVEAU, C. & CHHABRA, A. B. 1990 Two-point statistics of multifractal measures. *Physica* A **164** (3), 564–574.

MENEVEAU, C. & MARUSIC, I. 2013 Generalized logarithmic law for high-order moments in turbulent boundary layers. *J. Fluid Mech.* **719**, R1.

MENEVEAU, C. & SREENIVASAN, K. 1991 The multifractal nature of turbulent energy dissipation. *J. Fluid Mech.* **224**, 429–484.

MONIN, A. & YAGLOM, A. 2007 Statistical fluid mechanics: mechanics of turbulence. Volume II. Translated from the 1965 Russian original.

O'NEIL, J. & MENEVEAU, C. 1993 Spatial correlations in turbulence: predictions from the multifractal formalism and comparison with experiments. *Phys. Fluids* A **5** (1), 158–172.

PERRY, A. & CHONG, M. 1982 On the mechanism of wall turbulence. *J. Fluid Mech.* **119**, 173–217.

PERRY, A., HENBEST, S. & CHONG, M. 1986 A theoretical and experimental study of wall turbulence. *J. Fluid Mech* **165**, 163–199.

POPE, S. B. 2000 *Turbulent Flows*. Cambridge University Press.

PRANDTL, L. 1925 Report on investigation of developed turbulence. *NACA Rep.* TM-1231.

SCHULTZ, M. P. & FLACK, K. A. 2007 The rough-wall turbulent boundary layer from the hydraulically smooth to the fully rough regime. *J. Fluid Mech.* **580**, 381–405.

DE SILVA, C., MARUSIC, I., WOODCOCK, J. & MENEVEAU, C. 2015 Scaling of second-and higher-order structure functions in turbulent boundary layers. *J. Fluid Mech.* **769**, 654–686.

SMITS, A. J., MCKEON, B. J. & MARUSIC, I. 2011 High-Reynolds number wall turbulence. *Annu. Rev. Fluid Mech.* **43**, 353–375.

TOWNSEND, A. 1976 *The Structure of Turbulent Shear Flow*. Cambridge University Press.

WOODCOCK, J. & MARUSIC, I. 2015 The statistical behaviour of attached eddies. *Phys. Fluids* **27** (1), 015104.